Nanoscale

Oriented attachment interfaces of zeolitic imidazolate framework nanocrystals

Journal:	*Nanoscale*
Manuscript ID	NR-COM-02-2023-000702.R1
Article Type:	Communication
Date Submitted by the Author:	25-Mar-2023
Complete List of Authors:	Han, Xiaocang; Shanghai Jiao Tong University, Su, Rui; Innovative Center for Advanced Materials, Hangzhou Dianzi University Chen, Wenqian; Shanghai University School of Environmental and Chemical Engineering, Han, Qi; Southern University of Science and Technology, Environmental Science and Engineering Tian, Yuan; Johns Hopkins University Han, Jiuhui; Tohoku University, Wang, Xiaodong; Shanghai Jiao Tong University, Song, Shuangxi; Shanghai Jiao Tong University Reddy, Kolan; Shanghai Jiao Tong University, State Key Laboratory of Metal Matrix, School of Materials Science and Engineering Deng, Hexiang; Wuhan University, Chemistry and Molecular Sciences Liu, Pan; WPI-AIMR, ; Shanghai Jiao Tong University, Chen, Mingwei; Johns Hopkins University, Materials Science and Engineering; Tohoku University, WPI-AIMR

COMMUNICATION

Oriented attachment interfaces of zeolitic imidazolate framework nanocrystals

Received 00th January 20xx,
Accepted 00th January 20xx

DOI: 10.1039/x0xx00000x

Xiaocang Han[a], Rui Su[b], Wenqian Chen[c,d], Qi Han[e], Yuan Tian[f], Jiuhui Han[c], Xiaodong Wang[a], Shuangxi Song[a], Kolan Madhav Reddy[a,c], Hexiang Deng[e], Pan Liu[a,c]*, Mingwei Chen[f]*

Understanding the growth and coarsening mechanisms of metal-organic framework (MOF) nanoparticles is crucially important for design and fabrication of MOF materials with diverse functionalities and controllable stability. Oriented attachment (OA) growth is a common manner of MOF nanocrystal coarsening and agglomeration but the underlying molecular mechanisms have not been well understood to date. Here we report the molecular-scale characterization of OA interfaces of zeolitic imidazolate framework (ZIF) crystals by the state-of-the-art low-dose aberration-corrector transmission electron microscopy. A series of OA interfaces with different molecular structures are captured, implying that multiple kinetic steps are involved into the OA growth of the ZIF crystals from non-directional physical attractions between primary nanocrystals, lattice-aligned attachment of the ligand-capped nanocrystals, to coherent interfaces with perfect lattice alignment or stacking-faults. It was found that the surface capping organic ligands not only play an essential role in crystal lattice alignment by near-field directional interactions, but also dominate the interfacial reaction kinetics by interfacial diffusion-controlled elimination of excess surface capping ligands. These observations provide molecular-scale insights into the OA growth mechanisms of ZIF crystals, which is important for engineering MOF crystal growth pathways by designing surface capping ligands.

Metal-organic frameworks (MOFs), consisted of metal nodes and organic linkers, are a class of organic-inorganic hybrid materials[1,2] with a high surface area and large porosity for a wide range of applications in photonics, electronics, catalysis, gas storage and separation[3–12]. The properties of MOF crystals can be greatly augmented by the co-aligned ensemble of polyhedral MOF nanoparticles with unique morphologies, symmetries, structures for on-demand functionality[13–18]. The crystal growth of MOFs by oriented attachment (OA) has been recognized as a common manner of coarsening in a wide range of synthetic systems and is of great importance for designing and fabricating MOF crystals with size-dependent attributes and enhanced physical and chemical properties[18–22]. Different from monomeric addition in classical crystal growth, the crystallization by OA proceeds via repeated attachments of crystalline nanoparticles on specific crystal facets that are lattice-matched. For its importance, the OA crystal growth has been extensively studied for various inorganic metal[23,24], metal oxide[25–27] and semiconductor nanomaterials[28–30], minerals[31,32], zeolites[33,34] and et al., in particular, using *in situ* transmission electron microscopy (TEM) [24,35,36], in past two decades[37–40]. For instance, it has been observed that the primary iron oxide nanoparticles approach and rotate to reach perfect alignment before attachment, jump to contact, and subsequently fuse into a single crystal[26]. For this case, direction-specific Coulombic interactions have been counted as the driving force for the jump to contact. In the view of thermodynamics, except the primary driving force of surface energy reduction[25,41,42], the non-covalent interactions of van der Waals (vdW) forces[27,43], Coulombic interactions[26], dipolar interactions[24], hydrogen bonding[44] and steric forces[35,45], can also play an important role in the OA crystal growth[46]. Compared to extensive discussions on atomic-scale dynamic process and driving forces for OA growth of inorganic materials, the molecular-scale details of attachment behavior and interfacial interactions for MOF crystals are barely reported and remain largely unknown[19,21,22,47]. This is mainly limited by the structural complexity, instability of MOFs[48] and insufficient spatial resolution of *in situ* TEM techniques[49–51].

Recently low-dose high-resolution TEM (HRTEM) combining with direct electron detection camera (DEDC) has been proven to be a powerful tool for characterizing MOFs structures by effectively minimizing the electron beam irradiation damage[52–54]. In this study we employed this advanced characterization tool to investigate the structures of OA growth {110} interfaces of zeolitic imidazolate framework (ZIF) crystals (ZIF-67 and ZIF-8), which provides rich information of phase transition, particle attachment, and device performance[55,56]. Both ZIF-67 and ZIF-8 have been the widely studied and attract considerable interests for potential

[a]*State Key Laboratory of Metal Matrix Composites, School of Materials Science and Engineering, Shanghai Jiao Tong University, Shanghai, 200240, People's Republic of China;*
[b]*College of Materials & Environmental Engineering, Hangzhou Dianzi University, Hangzhou 310018, People's Republic of China;*
[c]*Advanced Institute for Materials Research, Tohoku University, Sendai 980-8577, Japan;*
[d]*School of Environmental and Chemical Engineering, Shanghai University, Shanghai 200444, People's Republic of China;*
[e]*Key Laboratory of Biomedical Polymers-Ministry of Education, College of Chemistry and Molecular Sciences, Wuhan University, Wuhan 430072, People's Republic of China;*
[f]*Department of Materials Science and Engineering, Johns Hopkins University, Baltimore, MD 21218, USA.*

applications in gas storage and catalysis owing to their high permanent porosity and high thermal and chemical stability[57,58]. ZIF-8 and ZIF-67 have a sodalite body-centered cubic structure (space group *I-43m*) which is constituted by Zn/CoN_4 tetrahedral nodes and 2-methylimidazolate (Hmim) ligands[7]. Our low-dose Cs-corrected HRTEM observations unveils a series of different OA interfacial structures from non-directional physical contact to lattice-aligned attachment and coherent interfaces with perfect lattice alignment or stacking-faults, suggesting that multiple kinetic steps are involved into the ZIF OA crystal growth (**Fig. 1a**).

ZIF-67 has a framework formula of [Co(2-methylimidazole)$_2$ or Co(mim)$_2$], and the nanocrystals examined in this work were synthesized by a hydrothermal method at room temperature and have regular rhombic dodecahedral morphology with the average size of ~50±5 nm (**Fig. 1b** and **Fig. S1**). The exposed {110} surface facets of the rhombic dodecahedral crystals can be readily observed in HRTEM images taken along a <111> axis. The topmost surfaces usually have a zigzag termination which is constructed by close cages and a topmost Co^{2+} ion with 3 out of 4 solvated mim^- linkers bonding with neighboring Co^{2+} ions and one dangling neutral monodentate Hmim linker (**Fig. S2**). The nanocrystals are capped by Hmim species to maintain charge neutrality and local tetrahedral configuration[59]. The low-magnification TEM image (**Fig. 1b**) shows apparent assemblies of co-aligned ZIF-67 nanocrystals with various {110} OA interfaces along 1D and 2D directions. In fact, the formation of the assembled crystals provides the direct evidence that the OA growth of ZIF-67 nanocrystals takes place *via* the {110} facet-to-facet attachment as illustrated in **Fig. 1c**. We found that the OA coalescence produces a series of interfaces from fully coherent to defective ones, which are associated with lattice alignment and interfacial reactions. To form a seamless transitional contact between primary ZIF-67 nanocrystals, the misalignment angle cannot be larger than ~8.2 degree even the particles are close enough and partially contact as indicated by red arrows.

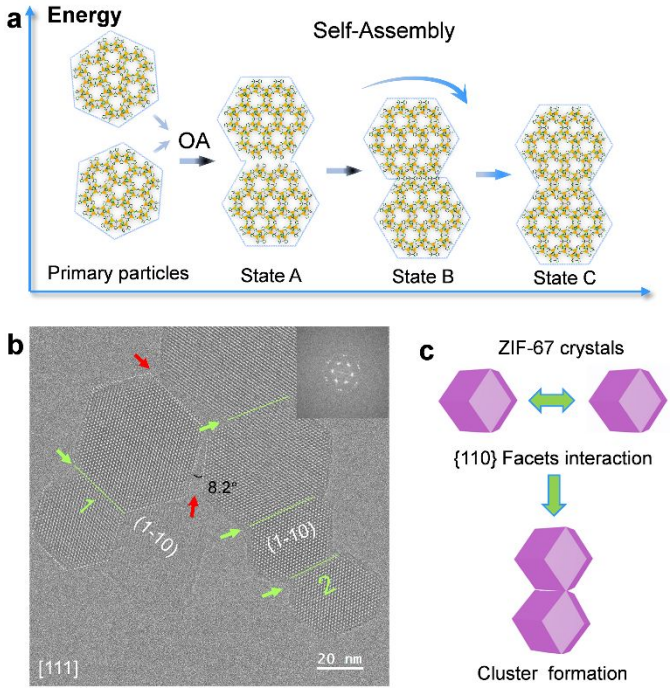

Fig.1 Super-nanoparticle assembly of MOF nanocrystals formed by oriented attachment. (a) A cartoon to describe the multiple steps of OA. (b) Low-magnification TEM image of a group of six attached ZIF-67 nanocrystals with very similar crystallographic orientations. The insert is the corresponding FFT pattern. (c) Schematic diagram showing the {110} facet-to-facet assembly of ZIF-67 nanocrystals. The seamless and seamed interfaces between assembly units were indicated by the green arrows and red arrows, respectively. The red arrows highlight the misorientation between the assembled particles as the degree of 8.2°.

Fig. 2a shows a seamless transitional interface. The lattice continuity is well reserved at the interface without noticeable interfacial defects in the HRTEM image (**Fig. 2b**). By the attachment of the zigzag {110} terminal surfaces of two crystals, the (1-21), (1-10) and (01-1) lattice planes of these two crystals are perfectly aligned with each other across the interface (**Fig. 2c**). Moreover, visible interplanar translation and grains rotation cannot be detected by the geometric phase analysis (GPA) (**Fig. 2d**). Consequently, the perfect continuity of the lattice leads to the formation of a large single crystal by OA of two individual crystals. The fully coherent interface indicates that the assembly of ZIF-67 crystals is unlikely driven solely by non-directional van der Waals forces. Instead, short-range interactions, together with chemical reactions and mass transport, are involved into the formation of the perfect interface with full coordination by forming chemical bonds between topmost atoms of the two attached surfaces. Since the topmost surfaces of the zigzag termination are capped by a layer of Hmim ligands, the

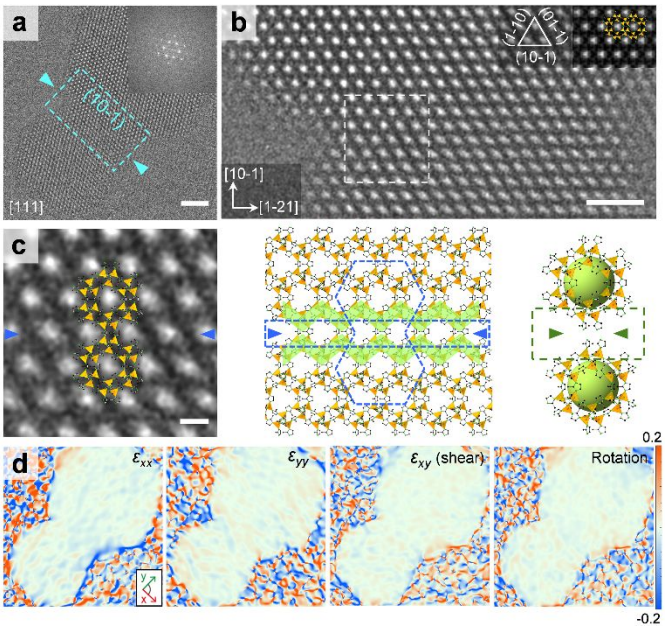

Fig.2 Coherent {110} interface structures of two-assembled ZIF-67 crystals. (a) The low-magnification TEM image of two perfect oriented attached ZIF-67 crystals taken along [111] axis extracted from the interface 1 in Fig. 1a. The insert is the corresponding FFT pattern. (b) Wiener-filtered HRTEM images of cyan box region in (a) overlaid with the simulated image and projected cages model in the right inset. (c) Enlarged HRTEM images of white box region in (a) with corresponding interface structure model (in middle part) projected along [111] axis. The zigzag-to-zigzag {110} interfacial structure with regard to two self-assembled crystals showing the perfect arrangement of molecular species as they do in internal structure. Two attached surface planes are linked by a single line of mim ligands denoted by blue dashed frame and arrows. Right, non-chemical bonding between two approaching cages marked by green frame and arrows, indicating that chemical bonding involved at perfect interface sharing a single layer of ligands. (d) Corresponding ε_{xx}, ε_{yy}, ε_{xy} and rotation strain maps of (a) rendered in color codes. Scale bars in (a, b, c) are 10, 5 and 1 nm. Cage models: orange is ZnN_4 tetrahedra, black and green represent C and N atoms, respectively (H atoms are omitted for clarity).

extra layer of Hmim ligands from one crystal surface must be expelled during OA growth in order to form a perfect interface (**Fig. 2c**). From the comparison between the free {110} surfaces with the zigzag termination and the full coherent {110} OA interfaces, one can find that chemical reactions and diffusion are the essential steps for the perfect interface formation. These processes may include the breaking of the bindings between Hmim and Co ions at the interface and the subsequent expulsion of Hmim ligands for forming new metal-ligand coordination. Similar to the ZIF-67, the fully coherent {110} OA interfaces are also observed in the ZIF-8 nanocrystals with a zigzag {110} surface termination (**Fig. S3**). Therefore, the kinetic process of the perfect interface formation could be common for isostructural ZIF-67 and ZIF-8 OA crystal growth with minimized interface energies.

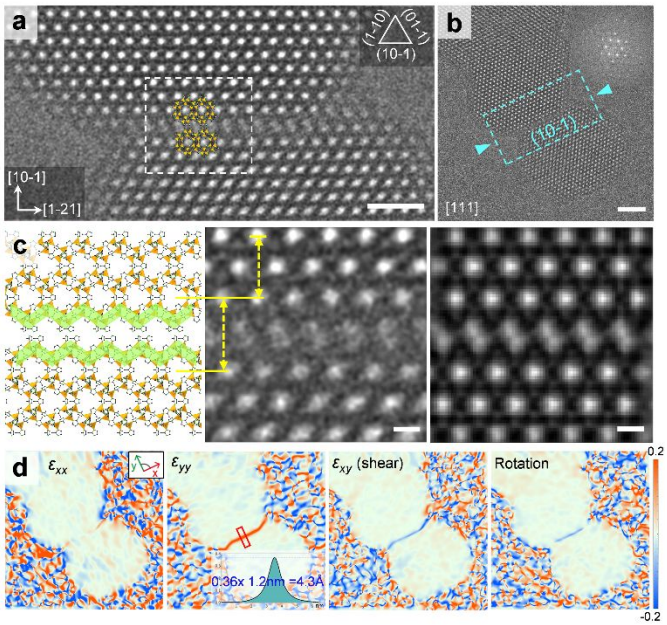

Fig. 3 Defective {110} interface with a spacer layer between two assembled ZIF-67 crystals. (a) Wiener-filtered HRTEM image of cyan box interface region in (b) along [111] direction inserted with projected cages model. (b) The low-magnification TEM image of two nearly perfect oriented attached ZIF-67 crystals taken along [111] axis extracted from the interface 2 in Fig. 1a. The insert is the corresponding FFT pattern. (c) Projected structural model, experimental and simulated images of ZIF-67 {110} interface viewed along the [111] axis. The enlarged and denoised HRTEM image of white dashed frame in (a). (d) Corresponding ε_{xx}, ε_{yy}, ε_{xy} and rotation strain maps of (b) rendered in color codes. Quantitative lattice strain at interface was inserted in εyy map. The vertical stacking displacement along (1-21) plane at the interface is denoted by double cyan arrows line shown in (c). Scale bars in (a, b, c) are 5, 10 and 1 nm.

In addition to the fully coherent OA interfaces, we noticed that some interfaces have obvious defects from imperfect OA growth. These defective interfaces, in fact, provide additional information on the OA kinetics of ZIF crystals. The HRTEM image (**Fig. 3a**) along the [111] axis displays a defective OA interface of ZIF-67 crystals where an extra molecular layer between two attached {110} surfaces can be observed. The denoised HRTEM image clearly shows that the two attached (110) surfaces from the upper and lower crystals have a zigzag termination (**Fig. 3c** and **Fig. S4**). The (1-10) and (01-1) lattice planes of these two crystals are well aligned across the interface without rotating or tilting, but the continuity of the lattice stops at the extra layer (**Fig. 3c**). On the zigzag (110) surfaces of ZIF-67 crystals, the

capping monodentate Hmim species have the height of 2.2 Å and contain no coordination bonds in the direction parallel to the crystal surface. Based on the molecular-scale HRTEM images and the structure of the zigzag (110) termination, we constructed the structure model of the defective {110} OA interface by the direct attachment between two Hmim-capped zigzag (110) surfaces of ZIF-67 crystals. The model is verified by the consistency between the experimental HRTEM image and the simulated one of the interface model (**Fig. 3c**). The degree of the separation between two crystals can be accurately determined by lattice spacing measurements. The vertical and horizontal displacements of the upper crystal with respect to the lower one are 4.33 Å and 2.25 Å, respectively (**Fig. 3c** and **Fig. S5**). Again, these displacements are well consistent with the structure model with one extra layer of surface ligands from the direct contact of two monodentate Hmim species capped zigzag (110) surfaces by following the stacking sequence of (10-1) lattice planes as -B-A-B-A- (**Fig. S5**). The separation degree (along the normal of the interface) between crystals relative to a perfect single crystal can be more accurately determined by GPA of the raw HRTEM image (**Fig. 3b**). The lattice strains along [1-21] (ε_{xx}) and [10-1] (ε_{yy}) directions, shear strain (ε_{xy}) as well as rotation are shown in **Fig. 3d**. In contrast to the negligible strains of ε_{xx}, the obvious ε_{yy} and ε_{xy} strains suggest the uniform lattice displacements along [10-1] directions and the shear component along the interface. All the lattice strains are exactly localized at the narrow interface region with a full width at half maximum (FWHM) of 9.1 Å and no long-range strains out of the interface can be seen (**Fig. 3d**, insert), demonstrating the attachment is held by a short-range molecular interaction between the two topmost Hmim capping layers. Generally, nanoscale interactions guiding the self-assembly of MOFs are associated with vdW forces, dipole-dipole interactions, hydrogen bonding and steric force[20–22]. The fact that the defective interface with an extra Hmim spacer layer can realize nearly perfect lattice alignment of ZIF-67 nanocrystals along the out-of-surface direction implies that there may be a relatively long-range directional interaction, beyond the thickness of the extra organic ligand layer, which can represent the lattice periodicity to bring two nanocrystals together for perfect lattice alignment. Although the vdW forces can act over long distance and may play certain roles in attracting the two crystals approaching each other [17,20–22], the non-directional nature is not expected to give excellent lattice alignment. We noticed that the interfacial displacement of 4.33 Å along [10-1] corresponds to the thickness of the extra ligand layer (2.2Å) and the interlayer distance (~2.1 Å) between two capping ligand layers. This suggests the direct adhesion of two ligand-terminated surfaces without chemical reactions. Therefore, the interaction between Hmim ligands capping on the surfaces of two attached particles may play a decisive role in the particle binding [20,35], most likely by hydrogen (N-H···N) bonds between terminal Hmim on one nanoparticle and the surface mim^- on the paring nanoparticle (**Fig. S6**). This hypothesis is supported by the distance between uppermost nitrogen atoms along the (01-1) plane which is close enough (3.09 Å) for hydrogen. Besides, two possible adding positions of proton H on solvated mim^- ions

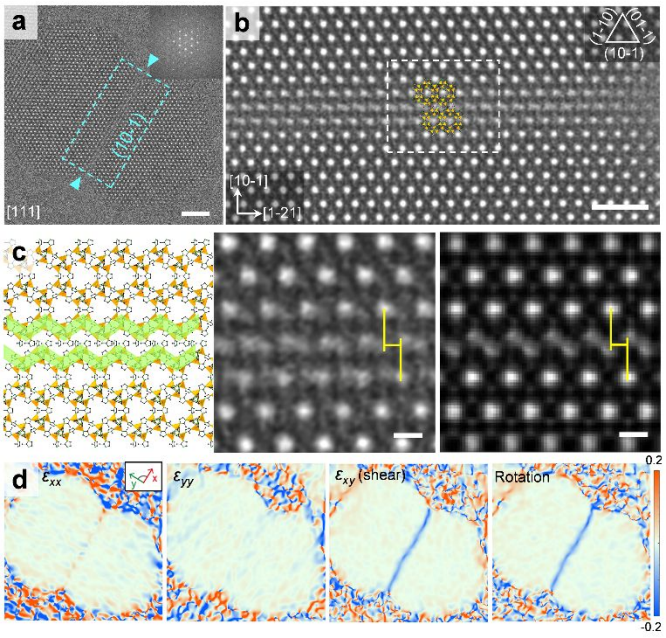

Fig. 4 Incoherent {110} interface with stacking fault. (a) The low-magnification TEM image of two close oriented attached ZIF-67 crystals taken along [111] axis. The insert is the corresponding FFT pattern. (b) Wiener-filtered HRTEM images of cyan box interface region in (a) inserted with projected cages model. (c) Projected structural model, experimental and simulated images of ZIF-67 {110} interface viewed along the [111] axis. The enlarged and denoised HRTEM image of white dashed frame in (a). (d) Corresponding ε_{xx}, ε_{yy}, ε_{xy} and rotation strain map of (a) rendered in color codes. Scale bars in (a, b, c), 10, 5 and 1 nm.

match with the hydrogen bonding angles. While, the other cases (<135°) can be excluded from the experience value of hydrogen bonding (**Fig. S6**). Capping ligands thus mediates the alignment of the nanocrystals along specific crystallographic directions through the formation of inter-particle hydrogen bonds, illustrating how local interactions, such as hydrogen bonding, can play a major role in crystal alignment in OA growth.

In addition to the defective OA interfaces with an extra ligand layer, we found that OA growth of ZIF-67 nanocrystals can generate stacking faults at OA interfaces by lattice shift along <121> direction. **Fig. 4a** shows a low magnification HRTEM image of an OA interface in which the lattice continuity breaks at the interface. The zoom-in image (**Fig. 4b**) shows the lattice breaking is caused by a displacement along [1-21] on (10-1) OA interface between the upper and lower crystals while there is no vertical displacement along [10-1] direction. The shift distance is measured to be 6.8 (±0.75) Å (**Fig. 4c** and **Fig. S7**), which is nearly equal to the {121} interplanar spacing (6.9 Å) of ZIF-67. Based on the HRTEM image, we built a molecular model to describe the defective interface. The simulated HRTEM image from the structural model is well consistent with the experimental one (**Fig. 4c**), demonstrating the key structural features of the OA interface have been captured by the interfacial structure model. In fact, the mis-alignment between the upper and lower crystals leads to the stacking sequence change of the (10-1) lattice planes from -B-A-B-A- to -B-A-A-B- at the OA interface (**Fig. S7**). To study the interfacial translation

and rotation at this stacking-fault interface, we conducted the GPA analysis of **Fig. 4a**. The distributions of lattice strains along [1-21] ($\varepsilon_{xx,}$ parallel to the interface) and [10-1] (ε_{yy}, normal to the interface) directions as well as shear strain (ε_{xy}) and rotation are shown in **Fig. 4d**. In contrast to the apparent shear composition in ε_{xy} map, the negligible ε_{xx} and ε_{yy} suggest no obvious normal lattice displacements at the OA interface. The shear strain ε_{xy} at the interface further supports that the defective OA interface defect can be described by the stacking fault and is formed by the shear displacement along the [1-21] direction on the (10-1) lattice plane.

To uncover the ligand related mechanisms of OA attachment, it is necessary to compare the relative energy difference between possible OA interface configurations. Due to the lack of Co parameters in the "3ob" set, we used the ZIF-8, which has the similar crystal structure as ZIF-67, as the model system. Since interface energies are mostly dominated by hydrogen or vdw interactions between the organic part of ZIFs, the structure difference between ZIF-8 and ZIF-67 will not obviously affact the relative energy difference from the calculations. Here all under-coordinated Zn sites are capped by Hmim ligands. The optimized interface structures are illustrated in **Fig. S8**. We considered the direct attached one with gap as AA stacking, cross matched one without gap as AB stacking in the body-centered cubic crystal, cross one with gap as AB' stacking, where upper layers shift half of the cage distance along horizontal direction. It was found that the stacking-fault OA interface observed by HRTEM (**Fig. S8c**) is a partially relaxed interface formed by the direct contact of two Hmim-ligand capped (110) surfaces. The arrangements of zigzag Co trimers and capping ligands on the stacking fault plane are spatially staggered, suggesting the direct adhesion of two ligand-terminated surfaces without chemical reactions. We calculated the interplanar binding energy difference of AA and AB' with AB configurations as $\Delta E = (E_{AA}\ or\ E_{AB'} - E_{AB})/A$, where E_{AA}, $E_{AB'}$ and E_{AB} are energies of density functional tight-binding (DFTB) relaxed interface configurations and A is the surface area of interface. Our calculation shows that the AA or AB' configurations are 0.051 J/cm^2 and 0.064 J/cm^2 higher than the AB configuration, respectively. So, compared to the cross one, the imperfect OA attachment with hydrogen bonding should be energetically favorable. Owing to the complexity of the adsorbing molecules or large surface tension with a small crystal size, the optimized direct attached interface model (**Fig. S8a**) is a little different from but very close to the defective interface in **Fig. 3** (**Fig. S9**). For the coarsening process of nanocrystals capped with organic ligands, the nanoparticles would experience a short-range barrier due to steric repulsion and ligands expulsion reactions before undergoing perfect attachment[35]. Except for perfect interface, the stacking fault interface is the most energetically stable attachment configuration, attributed to its smallest spatial overlap and closest distance of two surfaces. Thus, it is reasonable to deduce that the stacking-fault interfaces could be another way of OA growth transformed by one of the directed attached particles by shifting along <010> direction without ligands expulsion reactions. The growth of MOF crystal is closely related to the crystal orientations, local liquid surroundings, growing temperatures, so on. Even under a single set of synthetic conditions, multiple growth modes, such as Ostwald ripening and particle attachment, may take place due to the variation of local chemical and physical environments. Since this is the postmortem observation, we do not know the exactly local growth environment and growth rate of the resulting MOF crystals. However, the extremely unstable attached crystals would like to move apart by ultrasound used for preparing TEM samples. The attached configurations we observed are most like in the latter stage of the attachment growth and are in a metastable or stable state.

In previous studies, the molecular-scaled OA reactions of MOF nanocrystals cannot be directly resolved, which is limited by both spatial and temporal resolutions of *in situ* TEM. As a result, the kinetic processes are mainly described by morphology changes of nanoparticles. The atomic- and molecular-scale physical and chemical characteristics within interfacial regions that govern alignment and attachment reactions have not been revealed by direct experimental observations. During OA crystal growth, attractive long-range interactions could dominate and draw dispersed nanoparticles into a close range where short-range interactions between specific facets work and crystal alignment is manipulated by near-field directional interactions that can represent lattice periodicity, such as the hydrogen bonding from the capping Hmim ligands on the extending {110} surface of ZIF-67 crystals. For the ZIF crystals, the crystal alignment by hydrogen interactions could be an essential kinetic step of the OA growth process of MOF crystals. This assumption is well in line with our observation of the defective OA interfaces with a spacer layer and previous observations in ZIF-8 crystals[20]. The interfacial interactions between crystals, depending on their mutual crystallographic alignment, are responsible for further attraction to establish low-energy interfacial configurations. Based on different synthetic conditions, it has been suggested that the unsaturated surface Co sites could also be capped by solvent species which is hardly to be distinguished for the weak contrast in TEM images[20,60]. For the ZIF crystals, the capping Hmim ligands (maybe solvent species as well) contribute to the primary crystal alignment and attachment through the formation of interfacial hydrogen bonding (**Fig. S9**). But, they may also affect the formation of a perfect lattice configuration with new full metal-ligand coordination since the chemical reaction process requires the elimination of an excess layer of Hmim species (maybe solvent species as well) from OA interfaces. The diffusion of Hmim ligands (maybe solvent species as well) could be the kinetically controlling step of the OA crystal growth of ZIFs. Thus, it could be the possible kinetic reason that the stacking fault OA interfaces are formed by the direct contact of two ligand capping surfaces without sluggish interfacial fusion by chemical reactions and interfacial diffusion.

Conclusions

In summary, we have successfully characterized the zigzag surface-mediated OA interfaces of ZIF-67 and ZIF-8 crystals by

employing a low-dose Cs-corrected HRTEM. The observations of defective interfaces provide compelling evidence that the self-assembly of ZIF crystals involves multiple kinetic steps from non-directional physical attractions to establish short-range surface-surface interactions by hydrogen bonding for crystal alignment. The formation of low-energy interfacial configurations take place by chemical reactions with the elimination of adsorbed species from OA interfaces or direct contact by forming stacking faults. These experimental observations provide new insights into the OA growth of ZIF crystals and may pave a new way in engineering MOF crystal growth by designing surface structures and surface capping organic ligands.

Author Contributions

M. C. and P. L. designed the project and guided the research. X. H. and P. L. performed the low-dose spherical aberration corrected HRTEM experiments. R. S. conducted the interface energy calculation. W. C. and Q. H. synthesized the ZIF-8 and ZIF-67 samples. H. D. supervised the ZIF-67 sample preparation. Y. T., J. H., X. W., S. S. and K. M. R. contributed to the HRTEM measurements. X. H., P. L. and M. C. interpreted the data and wrote the manuscript. All authors contributed to the extensive discussions of the results.

Acknowledgements

This work was supported by National Natural Science Foundation of China (Grant No. 52173224, 51821001, 52130105), Natural Science Foundation of Shanghai (No. 21ZR1431200, 23ZR1431500). P. L. is supported by the Program for Professor of Special Appointment (Eastern Scholar) at Shanghai Institutions of Higher Learning. Y. T. and M. C. is sponsored by the Whiting School of Engineering, Johns Hopkins University and National Science Foundation (NSF DMR-1804320).

Conflicts of interest

The authors declare no competing financial interests.

Notes and references

1 H. Li, M. Eddaoudi, M. O'Keeffe and O. M. Yaghi, *Nature*, 1999, **402**, 276–279.
2 O. M. Yaghi, M. O'Keeffe, N. W. Ockwig, H. K. Chae, M. Eddaoudi and J. Kim, *Nature*, 2003, **423**, 705–714.
3 H. Furukawa, K. E. Cordova, M. O'Keeffe and O. M. Yaghi, *Science*, 2013, **341**, 1230444.
4 L. E. Kreno, K. Leong, O. K. Farha, M. Allendorf, R. P. Van Duyne and J. T. Hupp, *Chem. Rev.*, 2012, **112**, 1105–1125.
5 V. Stavila, A. A. Talin and M. D. Allendorf, *Chem. Soc. Rev.*, 2014, **43**, 5994–6010.
6 J. Lee, O. K. Farha, J. Roberts, K. A. Scheidt, S. T. Nguyen and J. T. Hupp, *Chem. Soc. Rev.*, 2009, **38**, 1450–1459.
7 R. Banerjee, A. Phan, B. Wang, C. Knobler, H. Furukawa, M. O'Keeffe and O. M. Yaghi, *Science*, 2008, **319**, 939–943.
8 N. L. Rosi, J. Eckert, M. Eddaoudi, D. T. Vodak, J. Kim, M. O'Keeffe and O. M. Yaghi, *Science*, 2003, **300**, 1127–1129.
9 G. Férey, *Chem. Soc. Rev.*, 2008, **37**, 191–214.
10 H. Li, K. Wang, Y. Sun, C. T. Lollar, J. Li and H. C. Zhou, *Mater. Today*, 2018, **21**, 108–121.
11 S. Horike, S. Shimomura and S. Kitagawa, *Nat. Chem.*, 2009, **1**, 695–704.
12 K. Sumida, D. L. Rogow, J. A. Mason, T. M. McDonald, E. D. Bloch, Z. R. Herm, T.-H. Bae and J. R. Long, *Chem. Rev.*, 2011, **112**, 724–781.
13 N. Sikdar, M. Bhogra, U. V. Waghmare and T. K. Maji, *J. Mater. Chem. A*, 2017, **5**, 20959–20968.
14 S. Furukawa, J. Reboul, S. Diring, K. Sumida and S. Kitagawa, *Chem. Soc. Rev.*, 2014, **43**, 5700–5734.
15 A. Carné-Sánchez, I. Imaz, K. C. Stylianou and D. Maspoch, *Chem. - A Eur. J.*, 2014, **20**, 5192–5201.
16 T. Tsuruoka, S. Furukawa, Y. Takashima, K. Yoshida, S. Isoda and S. Kitagawa, *Angew. Chem. Int. Ed.*, 2009, **48**, 4739–4743.
17 S. Melinda, Y. Nobuhiro, J. Ah-Young and S. Granick, *Acc. Chem. Res.*, 2014, **47**, 459–469.
18 C. Avci, I. Imaz, A. Carné-Sánchez, J. A. Pariente, N. Tasios, J. Pérez-Carvajal, M. I. Alonso, A. Blanco, M. Dijkstra, C. López and D. Maspoch, *Nat. Chem.*, 2018, **10**, 78–84.
19 Y. Wang, L. Li, H. Liang, Y. Xing, L. Yan, P. Dai, X. Gu, G. Zhao, X. Zhao and S. Information, *ACS Nano*, 2019, **13**, 2901–2912.
20 Y. Zhu, J. Ciston, B. Zheng, X. Miao, C. Czarnik, Y. Pan, R. Sougrat, Z. Lai, C. E. Hsiung, K. Yao, I. Pinnau, M. Pan and Y. Han, *Nat. Mater.*, 2017, **16**, 532–536.
21 N. Yanai, M. Sindoro, J. Yan and S. Granick, *J. Am. Chem. Soc.*, 2013, **135**, 34–37.
22 N. Yanai and S. Granick, *Angew. Chem. Int. Ed.*, 2012, **51**, 5638–5641.
23 A. Halder and N. Ravishankar, *Adv. Mater.*, 2007, **19**, 1854–1858.
24 H. G. Liao, L. Cui, S. Whitelam and H. Zheng, *Science*, 2012, **336**, 1011–1014.
25 R. L. Penn and J. F. Banfield, *Geochim. Cosmochim. Acta*, 1999, **63**, 1549–1557.
26 D. Li, M. H. Nielsen, J. R. I. Lee, C. Frandsen, J. F. Banfield and J. J. De Yoreo, *Science*, 2012, **336**, 1014–1018.
27 X. Zhang, Y. He, M. L. Sushko, J. Liu, L. Luo, J. J. De Yoreo, S. X. Mao, C. Wang and K. M. Rosso, *Science*, 2017, **356**, 434–437.
28 M. P. Boneschanscher, W. H. Evers, J. J. Geuchies, T. Altantzis, B. Goris, F. T. Rabouw, S. A. P. Van Rossum, H. S. J. Van Der Zant, L. D. A. Siebbeles, G. Van Tendeloo, I. Swart, J. Hilhorst, A. V. Petukhov, S. Bals and D. Vanmaekelbergh, *Science*, 2014, **344**, 1377–1380.
29 J. J. Geuchies, C. Van Overbeek, W. H. Evers, B. Goris, A. De Backer, A. P. Gantapara, F. T. Rabouw, J. Hilhorst, J. L. Peters, O. Konovalov, A. V. Petukhov, M. Dijkstra, L. D. A. Siebbeles, S. Van Aert, S. Bals and D. Vanmaekelbergh, *Nat. Mater.*, 2016, **15**, 1248–1254.
30 F. Huang, H. Zhang and J. F. Banfield, *Nano Lett.*, 2003, **3**, 373–378.
31 D. Li, J. Chun, D. Xiao, W. Zhou, H. Cai, L. Zhang, K. M. Rosso, C. J. Mundy, G. K. Schenter and J. J. De Yoreo, *Proc. Natl. Acad. Sci. U. S. A.*, 2017, **114**, 7537–7542.
32 N. Gehrke, H. Cölfen, N. Pinna, M. Antonietti and N. Nassif, *Cryst. Growth Des.*, 2005, **5**, 1317–1319.
33 Z. Sheng, H. Li, K. Du, L. Gao, J. Ju, Y. Zhang and Y. Tang, *Angew. Chem. Int. Ed.*, 2021, **60**, 13444–13451.
34 S. Kumar, Z. Wang, R. Lee Perm and M. Tsapatsis, *J. Am. Chem. Soc.*, 2008, **130**, 17284–17286.
35 C. Zhu, S. Liang, E. Song, Y. Zhou, W. Wang, F. Shan, Y. Shi, C. Hao, K. Yin, T. Zhang, J. Liu, H. Zheng and L. Sun, *Nat. Commun.*, 2018, **9**, 1–7.
36 H. Zheng, R. K. Smith, Y. W. Jun, C. Kisielowski, U. Dahmen and A. Paul Alivisatos, *Science*, 2009, **324**, 1309–1312.
37 J. J. De Yoreo, P. U. P. A. Gilbert, N. A. J. M. Sommerdijk, R. L. Penn, S. Whitelam, D. Joester, H. Zhang, J. D. Rimer, A. Navrotsky, J. F. Banfield, A. F. Wallace, F. M. Michel, F. C.

Meldrum, H. Cölfen and P. M. Dove, *Science*, 2015, **349**, aaa6760.
38 B. B. V. Salzmann, M. M. van der Sluijs, G. Soligno and D. Vanmaekelbergh, *Acc. Chem. Res.*, 2021, **54**, 787–797.
39 X. Li, X. Liu and X. Liu, *Chem. Soc. Rev.*, 2021, 2074–2101.
40 J. J. De Yoreo and N. A. J. M. Sommerdijk, *Nat. Rev. Mater.*, 2016, **1**, 1–18.
41 M. José-Yacamán, C. Gutierrez-Wing, M. Miki, D. Q. Yang, K. N. Piyakis and E. Sacher, *J. Phys. Chem. B*, 2005, **109**, 9703–9711.
42 W. Lv, W. He, X. Wang, Y. Niu, H. Cao, J. H. Dickerson and Z. Wang, *Nanoscale*, 2014, **6**, 2531–2547.
43 W. Lv, W. Huo, Y. Niu, Y. Zhu, Y. Xie, X. Guo and W. He, *CrystEngComm*, 2015, **17**, 729–733.
44 M. Raju, A. C. T. Van Duin and K. A. Fichthorn, *Nano Lett.*, 2014, **14**, 1836–1842.
45 U. Anand, J. Lu, D. Loh, Z. Aabdin and U. Mirsaidov, *Nano Lett.*, 2016, **16**, 786–790.
46 K. J. M. Bishop, C. E. Wilmer, S. Soh and B. A. Grzybowski, *Small*, 2009, **5**, 1600–1630.
47 K. M. Vailonis, K. Gnanasekaran, X. B. Powers, N. C. Gianneschi and D. M. Jenkins, *J. Am. Chem. Soc.*, 2019, **141**, 10177–10182.
48 J. Cravillon, S. Münzer, S. J. Lohmeier, A. Feldhoff, K. Huber and M. Wiebcke, *Chem. Mater.*, 2009, **21**, 1410–1412.
49 K. Gnanasekaran, K. M. Vailonis, D. M. Jenkins and N. C. Gianneschi, *ACS Nano*, 2020, **14**, 8735–8743.
50 J. P. Patterson, P. Abellan, M. S. D. Jr, C. Park, N. D. Browning, S. M. Cohen, J. E. Evans and N. C. Gianneschi, *J. Am. Chem. Soc.*, 2015, **123**, 7322–7328.
51 X. Liu, S. W. Chee, S. Raj, M. Sawczyk, P. Král and U. Mirsaidov, *Proc. Natl. Acad. Sci. U. S. A.*, 2021, **118**, e2008880118.
52 D. Zhang, Y. Zhu, L. Liu, X. Ying, C. E. Hsiung, R. Sougrat, K. Li and Y. Han, *Science*, 2018, **359**, 675–679.
53 X. Li, J. Wang, X. Liu, L. Liu, D. Cha, X. Zheng, A. A. Yousef, K. Song, Y. Zhu, D. Zhang and Y. Han, *J. Am. Chem. Soc.*, 2019, **141**, 12021–12028.
54 L. Liu, Z. Chen, J. Wang, D. Zhang, Y. Zhu, S. Ling, K. W. Huang, Y. Belmabkhout, K. Adil, Y. Zhang, B. Slater, M. Eddaoudi and Y. Han, *Nat. Chem.*, 2019, **11**, 622–628.
55 X. Qu, Y. He, M. Qu, T. Ruan, F. Chu, Z. Zheng, Y. Ma, Y. Chen, X. Ru, X. Xu, H. Yan, L. Wang, Y. Zhang, X. Hao, Z. Hameiri, Z. G. Chen, L. Wang and K. Zheng, *Nat. Energy*, 2021, **6**, 194–202.
56 H. L. Yuan, K. Wang, H. Hu, L. Yang, J. Chen and K. Zheng, *Adv. Mater.*, 2022, **34**, 2205715.
57 K. S. Park, Z. Ni, A. P. Côté, J. Y. Choi, R. Huang, F. J. Uribe-Romo, H. K. Chae, M. O'Keeffe and O. M. Yaghi, *Proc. Natl. Acad. Sci. U. S. A.*, 2006, **103**, 10186–10191.
58 U. P. N. Tran, K. K. A. Le and N. T. S. Phan, *ACS Catal.*, 2011, **1**, 120–127.
59 J. Cravillon, R. Nayuk, S. Springer, A. Feldhoff, K. Huber and M. Wiebcke, *Chem. Mater.*, 2011, **23**, 2130–2141.
60 X. Han, W. Chen, R. Su, Y. Tian, P. Liu, P. Guan, M. Luo, J. Han, X. Cao, M. Pan and M. Chen, *Nanoscale*, 2021, **13**, 13215–13219.